TRI-PP-80-4
Jan 1980

THE TRIUMF* STOPPED π-μ CHANNEL

N.M.M. Al-Qazzaz**, G.A. Beer,
G.R. Mason, A. Olin, R.M. Pearce

Physics Department, University of Victoria
Victoria, B.C., Canada V8W 2Y2

D.A. Bryman, J.A. Macdonald,
J.-M. Poutissou, P.A. Reeve

TRIUMF, Vancouver, B.C., Canada V6T 2A3

M.D. Hasinoff, T. Suzuki

Physics Department, University of British Columbia
Vancouver, B.C., Canada V6T 1W5

Submitted to Nuclear Instruments and Methods

* Operated by the University of Alberta, Simon Fraser University, the University of Victoria, and the University of British Columbia at Vancouver, British Columbia. Work supported in part by the Natural Sciences and Engineering Council of Canada.

** Present Address: Petroleum Engineering Department
ICOQ, Kirkuk, Iraq.

Abstract

The TRIUMF stopped π-μ channel (M9) is described and the measured optical parameters are compared with design values. Measured beam characteristics of pions and muons for several different momenta are reported for protons incident on Be and Cu production targets. A beam of cloud muons at the channel momentum, from π decays near the production target, has been obtained having a high stopping density and small spot size.

1. Introduction

A low energy π-μ beam has been developed at TRIUMF for use in nuclear, atomic, particle and solid state physics, and in chemistry. The momentum range 30 - 150 MeV/c is well suited for stopping experiments and the pion beam has been used as well for low energy scattering experiments. The various properties required by different experiments include high stopping density, small spot dimensions, low contamination by unwanted particles, special time structure, spin polarization (in the case of muons), and a variable momentum interval. The latter makes it possible to match the range of stopping particles to the thickness of the sample being studied.

At TRIUMF, pions are produced by an extracted beam of 500 MeV protons impinging on an external target. This paper describes the channel M9 used to collect secondary particles from a thick production target, and deliver them as a beam with the desired characteristics to an experiment. The mechanical layout and optics design of the channel will be summarized first, followed by a description of the various beams available from the channel.

2. General Description of the Channel

The proton beam of up to 100 μA from the TRIUMF 500 MeV cyclotron is incident on a water-cooled ladder assembly containing up to six targets of various materials and thicknesses. A 1 cm copper target is used for experiments which need a beam spot of small dimensions and which can tolerate relatively large electron impurity arising from conversion in the target of gammas from π^0 decay.

A 10 cm beryllium target is used for experiments which require the maximum available flux and lower electron contamination, but not optimum beam quality. The upper limit to the target thickness imposed by multiple scattering of the proton beam is 20 g/cm^2.

The M9 channel elements have been compactly installed to minimize the channel length as shown in fig. 1. The pion production cross section up to ∿ 150 MeV/c has been measured to be approximately isotropic[1]) while high energy neutrons are strongly forward peaked. The effect of π absorption in the thick target was calculated[2]) to be small at angles less than ∿ 135° for low pion momenta of 77 to 130 MeV/c. Therefore, the take-off angle of 135° was chosen for the advantage of retaining pion flux while reducing the high energy neutron contamination relative to forward angles by several orders of magnitude. Two other channels not discussed here come off the same production target at forward angles.

The two-bend concept was chosen to obtain an achromatic focus at F2 (see fig. 1) with controllable momentum acceptance ΔP/P, and to lower the transmission of the channel for neutrons from the production targets. The channel length of 8.4 m is sufficiently long to pass through the 6 m of concrete and steel shielding. The pion decay length varies from 3 to 9 m for momenta from 50 to 150 MeV/c.

The first two quadrupoles Q1, Q2 define the angular acceptance of the channel, and together with the first bending magnet B1 determine the ultimate momentum resolution of the channel. Q1, Q2 and B1 bring particles to a double focus F1 with momentum dispersion in the horizontal plane at the mid-point of the channel. At approximately this position a set of vertical and horizontal slits define, respectively, the vertical plane phase space acceptance and the momentum acceptance of the beam. The focal plane at F1 is inclined to the channel axis at an angle of only 8°, whereas the slits move at right angles to the axis.

The second bending magnet B2 and the following two quadrupoles Q4, Q5 form the symmetric second half of the channel, and bring the beam to focus F2 at the location of the stopping target. The quadrupole Q3, located in the middle section of the channel between the slits and B2, is used to make F2 achromatic to first order.

The first quadrupole Q1 was constructed using radiation-hard mineral insulated conductors[3]) and has a 20 cm aperture; the remaining elements are of conventional materials and have apertures of 25 cm for the dipoles and 30 cm for all quadrupoles. Quadrupoles Q2 to Q5 have spherically shaped pole pieces. With this design, the poles can be economically machined and the coils more simply wound. Although the resulting magnetic field distribution[4]) along the beam axis has no flat top and there is a significant twelve-pole integrated harmonic, these characteristics have not proved to be serious obstacles to tuning the channel.

In the momentum range of this channel, 30 - 150 MeV/c, multiple scattering of the beam in air could produce significant deterioration in beam quality. Therefore the beam line is evacuated and a 125 μm thick mylar exit window is used near the experiment location.

The vacuum system at the front end has been designed to be radiation resistant and to facilitate remote handling. The stainless steel vacuum pipe is connected to the target shielding block pipe with an all metal, remotely-operable indium vacuum seal. Removal of front-end components for servicing is achieved by operating a remote bellows-compressing mechanism at the vacuum coupling downstream of Q2, permitting the quad doublet to be rolled away from the target shielding block

on a bearing system. The doublet stand and associated vacuum pipe may then be lifted vertically without interference from the target block flange.

The B1 vacuum box is designed so that neutral and high-momentum particles from the production target pass straight through into the shielding, rather than be scattered down the channel. This straight-through leg has a window flange through which a TV camera can view a scintillator at the production target for proton beam tuning. Beside the camera is a lucite Cerenkov counter which is used to monitor the flux of conversion electrons arising from gammas from π^0 decay and provides a relative measure of the incident proton current. This monitor is used to optimize the tuning of the proton beam on the production target for maximum pion flux in the channel, while the channel parameters are held constant.

The channel magnets are controlled from a remote console containing a stable voltage supply and one ten-turn potentiometer for each element; a 0 - 5 volt reference voltage is sent to each power supply to control output current. Current stabilization is 0.1% for quadrupoles and 0.01% for dipoles. An additional master potentiometer permits one to scale a channel tuned at a particular momentum to another momentum with this single control. Read-back from each power supply is in the form of 0 - 5 volt level derived from a shunt on the output and is monitored visually with a digital voltmeter.

A microprocessor-based control system has been designed which will permit more sophisticated channel tuning in addition to monitoring and diagnostic capabilities and storage of pertinent beamline parameters. The prototype for this system is presently under development at TRIUMF.

3. Beam Optical Parameters

Most of the beam optical parameters were measured with the pion beam produced from the 1 cm long copper production target at T2. The pions were identified in the presence of equal momentum muons and electrons by time of flight. Fig. 2 shows a typical time-of-flight spectrum measured with respect to the proton pulse in the primary beam line. The measured and predicted optical characteristics of the channel included vertical plane magnification, angular acceptance, momentum resolution, dispersion and acceptance. Values for these quantities are shown in Table 1.

A focus was set up at F1 by having a small slit gap on the axis at F1, and making small adjustments to Q1 and Q2 to minimize the pion energy interval as measured at F2 by stopping them in a Ge(Li) counter. The detector time constant was kept short to include $\lesssim$ 1% of the $\mu \to e\nu\nu$ (τ = 2.2 μs) decay. The optimum settings for Q1 and Q2 were within 10% of the design values.

The momentum resolution of the channel is determined to first order by the dispersion-to-magnification ratio at F1. For a production target of 1 cm projected width, the calculated momentum resolution is 1.1% P. Estimates of the resolution were obtained from the Ge(Li) counter measurements and from range curves using a 6 mm thick stopping scintillator. In both cases the intrinsic instrumental resolution of the measurement was $\sim$ 2.5%, which when extracted from the overall measured resolution gave a value of the beam resolution of $\lesssim$ 2% P.

The dispersion from the production target (T2) to F1 was measured in two different ways: in the first method the change in the position of the time-of-flight peak of the pion distribution was measured as a function of slit position at F1; in the second method the energy of the pions was measured with a Ge(Li) counter. Both methods were calibrated against momentum by keeping the slit gap in a fixed position at F1 and varying the field in B1. Results from the two methods agreed within 10%. The measured dispersion (0.64 ± .01 cm/%P) can be found from the slope in fig. 3 and is lower than the theoretical dispersion of 0.78 cm/%P.

The momentum dispersion between F1 and F2 focus positions was measured with a small slit gap on the axis at F1. By varying the field in the first bending magnet, a source of variable momentum beam was, in effect, produced on axis at F1. Then, by measuring the horizontal displacement X of the beam with a multi-wire proportional chamber[5] at F2, the dispersion was found. Fig. 4 shows the measured X *versus* momentum; the non-linear shape results from second order chromatic aberrations (proportional to momentum squared). The data can be fit by a curve expressed as[6]:

$$X = R_{16} \left(\frac{\Delta P}{P}\right) + R_{166} \left(\frac{\Delta P}{P}\right)^2 \qquad (1)$$

where R_{16} = 1st order momentum dispersion, and
R_{166} = 2nd order chromatic aberration coefficient.

The quadrupole Q3 is used to make the channel achromatic by inverting the sign of the angular dispersion close to the midplane. To set up the achromatic condition experimentally, the field in Q3 was varied, and at each setting the position of the horizontal slit gap was varied. If the channel were achromatic at a particular Q3 setting, then the position of the beam at F2 would be independent of the slit position to first order. However, the substantial second order chromatic aberrations and strong vertical plane coupled aberrations complicated the procedure: for small vertical and horizontal plane slit gaps (0.5 cm), it was possible to limit the aberrations present to second order chromatic. Then the position X of the beam at F2, a function of the slit gap position at F1, was dependent only upon the linear first order dispersion plus a quadratic term due to the second order aberration. Q3 was varied until the F2 horizontal position was a symmetric parabolic function of slit position, meaning that the first order dispersion linear component had been reduced to zero. The results of this technique are shown in fig. 5. By fitting the data to a second order polynomial like eq. (1) the residual first order dispersion (0.01 ± 0.2 cm/%P) and the chromatic aberration coefficient [0.06 ± .004 cm/(%P)^2] were determined. These results verify the predicted zero residual first order dispersion, *viz.* an achromatic focus. The second order aberration, however, is a factor of two larger than the predicted value of 0.03 cm/(%P)^2.

It was not possible to measure the vertical plane magnification from the production target to F1 or F2, since it was not possible to vary the position of the production target. But by varying the vertical position of the slit gap at F1, and measuring the position of the beam at F2 it was possible to measure the vertical magnification between F1 and F2. The accuracy of the measurement was limited because the magnification is small and because the resolution of the multi-wire chamber used at F2, determined by the wire spacing of 3 mm, was significant compared with the vertical dimension of the image at F1 and F2 (see fig. 6). From the slope the measured magnification is -0.23 ± 0.03, while the theoretical magnification is -0.38.

The momentum acceptance of the channel was determined by measuring the flux at F2 as a function of the horizontal slit gap width at F1, shown by the solid curve in fig. 7. By numerically differentiating this function, shown by the dashed curve, and using the measured F1 dispersion, a momentum acceptance of $\frac{\Delta P}{P}$ = (14 ± 2)% FWHM or (30 ± 2)% FWTM was obtained. This compares well with the theoretical acceptance of 24%.

The maximum angular acceptance (Table 1) was deduced from the beam-phase space measurements using two pairs of wire chambers[5]) separated by 50 cm along the beam axis, the first pair located at F2. Each pair of chambers measured the (X,Y) coordinates. By taking differences between the pairs of chambers, the angular divergence of the particles was found. Time-of-flight data were also recorded event-by-event so that separate phase space plots for pions, electrons, and cloud muons could be constructed.

The effect of the production target geometry on the acceptance of the channel was checked by measuring the flux from two Be production targets of length 5 cm and 10 cm with the channel optimized for the 10 cm target at several momenta. The 10 cm to 5 cm flux ratio was ∿ 1.5, indicating that the overall acceptance of the channel is not uniform along the target length.

4. Beam Characteristics

4.1. PIONS

A comparison between measured and predicted pion beam parameters is summarized in Table 2. The agreement between the measured results and results of the Monte Carlo program REVMOC[7]) is quite good. Predictions from TRANSPORT[6]) are also included in Table 2; although TRANSPORT takes less computing time it gives poorer estimates for the beam parameters.

The effect of slit gap width at F1 (or momentum bite) on the beam emittances at F2 are shown in figs. 8 and 9. The emittances of the pion and electron beams are similar, as expected.

4.2. MUONS

It is convenient to distinguish the different types of muon beams in the channel by their origin. The most copious are the "cloud muons" which come from pion decay occurring at the position of maximum pion density, which is near the production target. These were first observed during initial beam tests in 1975.

The source size of the cloud muons, unlike the pions and electrons, is not well defined, and it is of interest to estimate it. By using the inverse of the first order channel matrix from production target to F2, the beam size at the production target can be calculated. As a test of the accuracy of the method, the calculated pion beam size should be the same as the production target. As can be seen in fig. 10a, comparison is good in the vertical plane for which a first order calculation is reliable. The discrepancy in the horizontal plane may be due to the effect of the significant higher order aberrations, which have not been included in the back projection. The results for the cloud muon beam are shown in fig. 10b. Based on the pion results, only the vertical dimension can be considered reliable. Further measurements of this kind are being considered.

The surprisingly small dimensions for the cloud muon spot size are discussed in detail by Tschalar[8]) and Tanabe[9]). Qualitatively the muon source strength from a single pion momentum P_π has the approximate form $\exp[-\lambda(P_\pi)r]/r^2$ at a distance r from the production target, where λ is the decay length of the pion, and r is large compared to the target dimensions. In addition to this r-dependence, the probability of a muon trajectory occurring is non-zero in the laboratory frame only in a cone centred on the pion trajectory with half angle less than

$$\theta = \tan^{-1}[\gamma_\pi^{-1}(\beta_\mu^2/(\beta_\mu^*)^2 - 1)^{-\frac{1}{2}}] \qquad (2)$$

where * indicates centre of mass for $P_\pi > 39.4$ MeV/c. At pion momenta between 77 and 130 MeV/c, θ is 31° to 17.6°, respectively. Muons originating in the cone centred on the channel axis and with half angle θ can be accepted, with decays directly on the axis having the largest probability of being accepted by the channel. The small cloud muon spot size and consequent high luminosity is a distinct advantage for small targets with detectors in close proximity.

There is a smaller number of muons from pion decays in the channel. Nonetheless, these muons are of interest in experiments requiring high spin polarization. Decays taking place down the channel from the production target present muon sources which are distributed both transversely and axially in the channel, and these muons have correspondingly poor spot sizes and timing.

The extreme values of muon momentum corresponding to exactly forward and backward decays are given by

$$P_\mu = \frac{1 \pm \beta_\mu \beta_\pi}{1 + \beta_\mu^*/\beta_\pi} \cdot P_\pi \qquad (3)$$

The momentum of muons decaying in the channel in the forward direction in the centre of mass can be seen by the above expression to partially overlap the pion momentum band when the channel is operating at a large momentum acceptance. Thus, forward muons can originate from the complete length of the channel with increasing likelihood with increasing momentum and in the region before the first bend the distinction between cloud and forward muons is ambiguous.

Forward muons can be separated from pions by differences in their ranges. Because of the low channel momentum and short decay length for pions, muons from backward decay in M9 are of too low intensity to be of general interest.

Positive pions stopping in the outer layer ($\sim$ 100 mg/cm^2) of the production target form a source of μ^+ [10]). The optical performance of these surface muons is essentially the same as that of the pions. This beam is in demand at TRIUMF for experiments stopping μ^+ in thin targets. No corresponding intense negative muon beam exists since negative pions stopping in the production target undergo nuclear capture and do not decay.

4.3. BEAM INTENSITIES

The beam intensity was measured at momenta of 77, 96, 120 and 135 MeV/c; some typical values are summarized in Table 3. Beam composition was determined from a time-of-flight spectrum for pions, cloud muons and electrons (see fig. 2).

The proton current was monitored by a Cerenkov counter which viewed the production target. The counter was calibrated for each target against the measured current of electrons stripped off the internal H^- beam of the cyclotron at the extraction stripper foil with appropriate corrections for the electron stripping efficiency and transmission losses.

The positive pion fluxes shown in Table 3 are consistent with pion production cross sections for 500 MeV protons measured[1]) at TRIUMF within the uncertainties in the cross sections ($\sim$ 10%), proton current normalization ($\sim$ 20%), and channel angular ($\sim$ 10%) and momentum acceptance ($\sim$ 15%).

The beam intensity as a function of midplane horizontal slit gap width is shown by the solid curve in fig. 7. The curve is a composite of data for both polarities, both production targets, and all momenta studied. The vertical bars indicate the range of the data over these varied conditions. Although there is no striking systematic variation of the curve with any of the above variables, the curve tends to rise more steeply with increasing momentum and more so with the Be target than the Cu target.

In addition to the beams described in Table 3, the surface muon beam (positive, 29.8 MeV/c) from M9 has a flux of up to 2×10^4 s^{-1} μA^{-1} and a luminosity of $\sim 10^3$ $s^{-1}\mu_A^{-1}$ cm^{-2} for collimated spots of 0.5 - 10 cm^2.

4.4. MUON POLARIZATION

The polarization of the muon beam at each momentum was measured by stopping the μ^+ beam in a 1.0 cm thick carbon target maintained in a transverse magnetic field of 250 gauss and observing the time dependence of the decay electrons in a single detector. The electron detector was a large NaI detector (46 cm ϕ × 51 cm) which allowed the measurement of the energy of the outgoing electrons with a resolution of $\sim$ 7.0% at 50 MeV (excluding target thickness contribution).

The beam polarization was obtained from the experimental data in the following way. The electron intensity data has the form $M_1(\beta) + \beta\bar{P}M_2(\beta)\cos\theta$, where θ is the angle between the electron velocity vector and the μ spin, β is the electron velocity in units of c, $\bar{P}$ is the polarization, and M_1 and M_2 are defined in reference 11. First the experimental energy resolution function at each energy was folded with $M_1(\beta)$ and $M_2(\beta)$, and the energy loss due to finite target thickness included to obtain the modified functions $M_1'(\beta)$ and $M_2'(\beta)$. Then $\beta\bar{P}M_2'(\beta)$ / $M_1'(\beta)$ was fitted to the ratio of the asymmetric part of the measured spectrum to the isotropic part in the energy range 30-50 MeV to determine the polarization $\bar{P}$. In this way the dependence of the polarization on the threshold of the electron detector was eliminated and also it was possible to use only the region of large positive asymmetry to determine the polarization quickly and accurately.

An example of a fit to the normalized electron asymmetry data obtained with a 96 MeV/c mixed forward and cloud μ beam (as used in an experimental run) is given in fig. 11.

Table 4 summarizes the polarization of various beams in M9 measured by this technique and, for the case of surface muons, by a more conventional method using plastic scintillators. At low momenta the polarization of the abundant cloud muons may be less than adequate for most

experiments concerned with polarization. It is non-zero for the following reason. The cloud muons at a given channel momentum P_μ originate from pions not with a single momentum P_π, but from a range of P_π. For $P_\pi < P_\mu$, the pion decay is predominantly forward in the centre of mass and the polarization in the case of μ^+ is positive. For $P_\pi > P_\mu$, the decay is backward and the polarization is negative. The numbers contributed from the ranges $P_\pi < P_\mu$ and $P_\pi > P_\mu$ differ because of the variation of decay length and the production cross section with P_π, and hence the net polarization of μ^+ is non-zero.

Corresponding negative muon polarizations have not been measured because the depolarization caused by the spin-orbit interaction in the μ^- cascade is not well known and therefore the residual polarization of the μ^- in the ground state of the atom cannot be accurately related to the polarization at the time of capture.

5. Summary

The low momentum π-μ channel (M9) at TRIUMF produces high stopping density beams of pions and cloud muons of both polarities over a momentum range of 30 - 150 MeV/c, in addition to a high luminosity surface μ^+ beam.

An extension[12]) including a crossed-field, velocity-filter particle separator is presently being added to the channel to produce clean muon beams of momentum $\lesssim$ 80 MeV/c with low pion and electron contamination.

Thanks are due to D.E. Lobb and L.P. Robertson for assistance in the design; to J.H. Brewer, D.F. Measday, K. Nagamine, M. Salomon, W.C. Sperry, J.S. Vincent and M.S. Dixit for assistance in channel tuning; to T.A. Hodges for designing the slits; and to E.W. Blackmore and the TRIUMF operations crew for their assistance.

REFERENCES

1) E.L. Mathie, M.Sc. Thesis, University of Victoria, 1976, unpublished. P.W. James, D.A. Bryman, G.R. Mason, L.P. Robertson, J.S. Vincent and T.R. Witten, University of Victoria TRIUMF Report VPN-75-1 (1975)

2) W.C. Sperry, University of Victoria TRIUMF Report VPN-71-2 (1971)

3) A. Harvey, Proc. 4th International Conference on Magnet Technology, Brookhaven, 1972, p. 456

4) T.R. Gathright *et al.*, University of Victoria TRIUMF Report VPN-74-3 (1974)

5) D. Bryman, J. Cresswell and R. Skegg, Nucl. Instr. and Meth. 141 (1977) 573

6) K.L. Brown and S.K. Howry, TRANSPORT/360, Stanford Linear Accelerator Center Report SLAC-91 (1970)

7) P. Reeve *et al.*, TRIUMF Report TRI-DN-77-6 (1977);
P. Kitching, TRIUMF Report TRI-71-2 (1971)

8) C.Tschalär, LAMPF Informal Report LA-7222-MS (1978)

9) K. Tanabe, Particle Accelerators 2 (1971) 211

10) A.E. Pifer, T. Bowen and K.R. Kendall, Nucl. Instr. and Meth. 135 (1976) 39

11) C. Bouchiat and L. Michel, Phys. Rev. 106 (1957) 170;
A.M. Sachs and A. Sirlin, Muon Physics, ed. V. Hughes and C.S. Wu, New York Academic Press (1975)

12) J.A. Macdonald, TRIUMF Design Note TRI-DN-79-5 (1979)

TABLE 1

M9 optical parameters

		Theory	Measured
Horizontal plane magnification	T2-F1	-0.63	–
	T2-F2	1.75	–
Momentum dispersion	T2-F1	0.78 cm/%P	0.64 ± 0.01 cm/%P
	F1-F2:		
	R_{16}(1st order)	1.34 cm/%P	1.18 ± 0.09 cm/%P
	R_{166}(2nd order)	0.01 cm/(%P)^2	-0.08 ± 0.03 cm/(%P)^2
Momentum resolution	F1	1.2% P	<2.4% P
Vertical plane magnification	T2-F1	-3.0	–
	T2-F2	1.14	–
	F1-F2	-0.38	-0.23 ± 0.03
Momentum acceptance		24% P FWTM	(14 ± 2)% P FWHM
			(30 ± 2)% P FWTM
Solid angle acceptance		18.5 msr	≲25 msr

TABLE 2

Comparison of theoretical and typical measured phase space parameters for pions.

	FWHM				FWTM			
	x (cm)	x' (mr)	y (cm)	y' (mr)	x (cm)	x' (mr)	y (cm)	y' (mr)
Measured (± 0.6 cm, ± 1.5 mr)	3.0	54	1.3	74	6.9	150	3.0	200
REVMOC (Monte Carlo)	5.0	60	.9	86	7.0	140	2.0	140
TRANSPORT (1st Order)	3.0	100	1.8	140	-	-	-	-

TABLE 3

Typical beam intensity and composition

Target	π Spot	Momentum (MeV/c)	POSITIVE Total Flux ($10^5 s^{-1} \mu A^{-1}$)	POSITIVE π:μ:e (%)	NEGATIVE Total Flux ($10^5 s^{-1} \mu A^{-1}$)	NEGATIVE π:μ:e (%)
10 cm	Δx ∿10 cm	77	10	77:8:15	4.2	40:5:55
Be	Δy ∿ 2 cm	96	18	84:8:8	5.5	65:5:30
		120	18	93:5:2	7.3	80:4:16
1 cm	Δx ∿ 4 cm	77	4.1	—	2.8	30:3:67
Cu	Δy ∿ 2 cm	96	9.4	77:7:16	4	49:3:48
		120	9.6	91:3:6	—	—
		135	10	94:3:3	—	—

Table 4

Measured μ-Polarization $\bar{P}$

	P_μ	$\bar{P}$	Midplane X-slits
Cloud	77 MeV/c	31.8 ± 3.0%	30 cm
	96	47.3 ± 3.0	30
	120	57.3 ± 3.0	30
		57.5 ± 4.0	5
	135	77.4 ± 3.0	10
Forward	135	93.0 ± 3.6	10
Cloud and forward	135	84.4 ± 0.5	10
Surface	29	> 80	

Figure Captions

Figure 1: Schematic layout of M9

Figure 2: Typical time of flight spectrum for positive particles of 96 MeV/c

Figure 3: Momentum dispersion at midplane dispersed focus (F1). The solid line is a linear fit to the data points shown with errors. (See Table 1.)

Figure 4: Momentum dispersion of the second half of the channel. The curve is a second-order fit to the data. (See Table 1.)

Figure 5: Achromaticity at the experimental focus F2. The curve is a second order fit to the data as described in the text.

Figure 6: Vertical magnification from F1 to F2. The solid curve is a linear fit to the data. (See Table 1)

Figure 7: The solid curve is the relative flux transmitted through the channel as a function of midplane horizontal slit gap. The vertical bars indicate the range of the data over both polarities, both production targets (1 cm Cu, 10 cm Be) and all momenta studied. The dashed curve is a numerical differentiation of the solid curve, from which the momentum acceptance of the channel is inferred using the midplane dispersion from figure 3.

Figure 8: Phase space at F2 for pions with the 1-cm Cu target and midplane slit gap = 0.5 cm. a) Horizontal, b) Vertical. The contour labels are fractions of maximum.

Figure 9: Phase space at F2 for pions with the 1-cm Cu target and midplane slit gap = 15 cm a) Horizontal b) Vertical. The contour labels are fractions of maximum.

Figure 10: Back projection of source size at production target for a) pions b) cloud muons as described in the text. The rectangle shows the physical size of the target. The contour labels are fractions of maximum.

Figure 11: Normalized decay electron asymmetry spectrum for the 96 MeV/c cloud plus forward-decaying muon beam. The solid curve is the theoretical prediction $\beta\bar{P}M_2^1(\beta)$ / $M_1^1(\beta)$ obtained by folding the isotropic and asymmetric parts of the spectrum individually with the experimental resolution function as described in the text. The normalization factor of 0.844 gives the muon beam polarization $\bar{P}$.

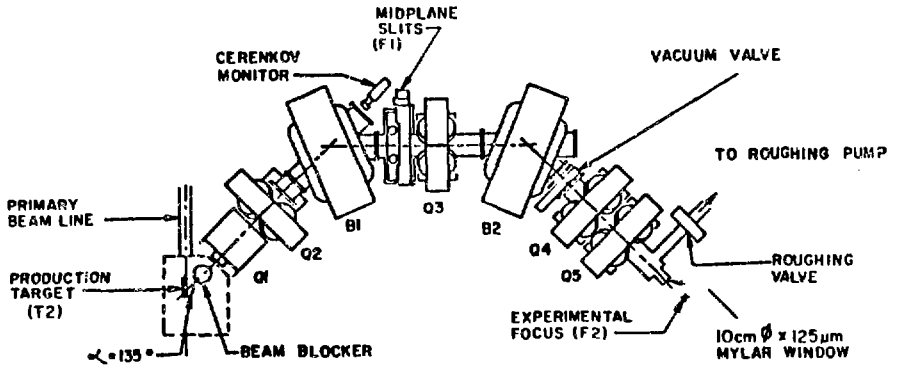

Fig. 1

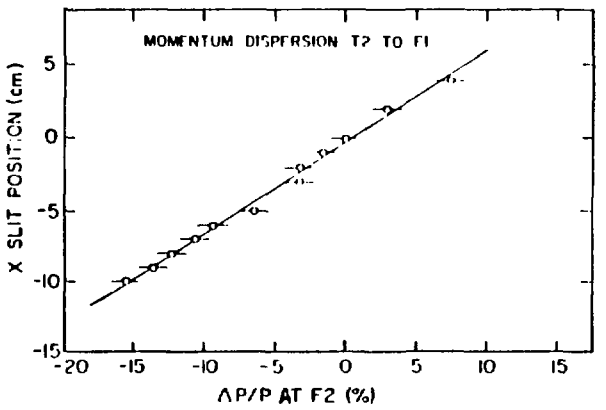

Fig. 3

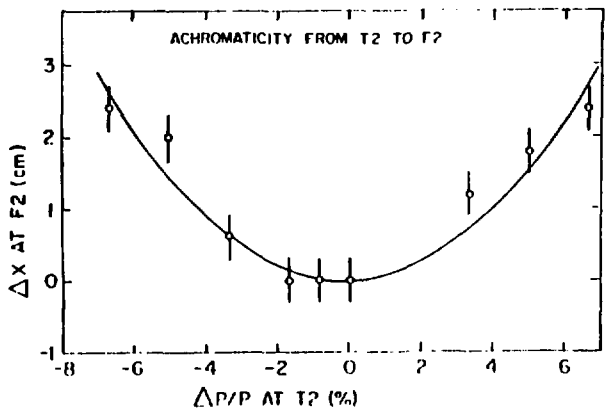

Fig. 5

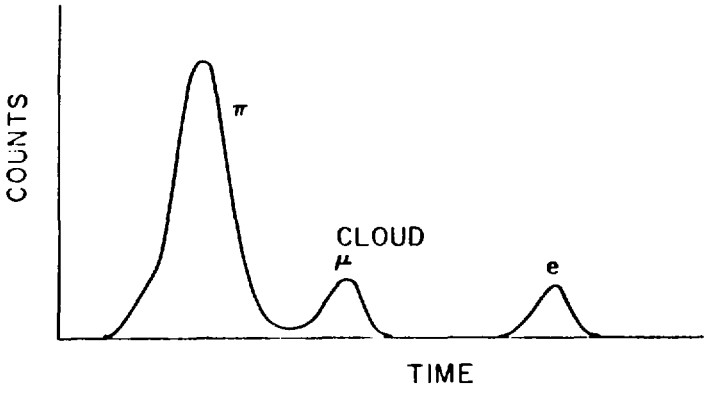

Fig. 2

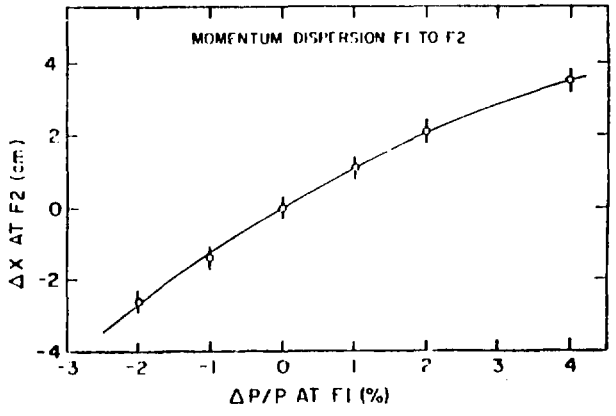

Fig. 4

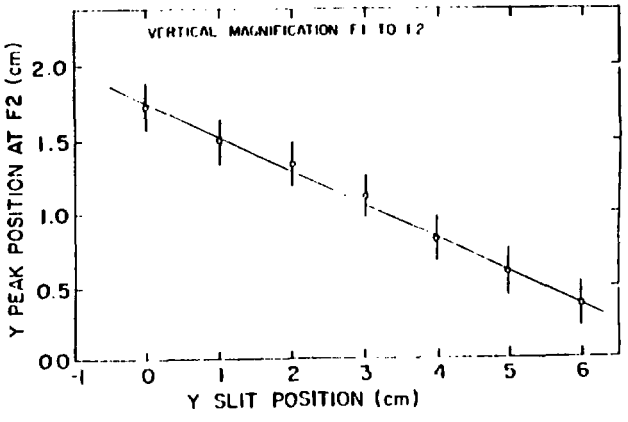

Fig. 6

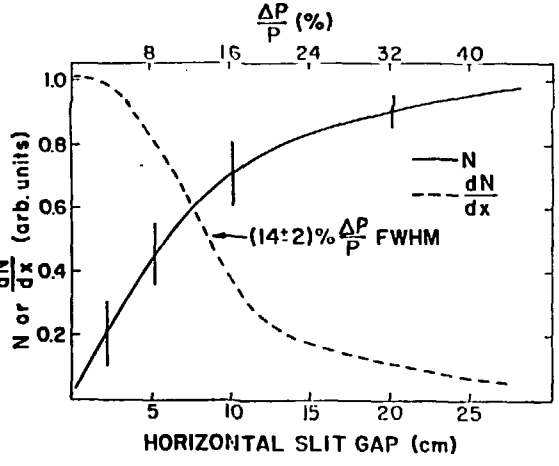

Fig. 7

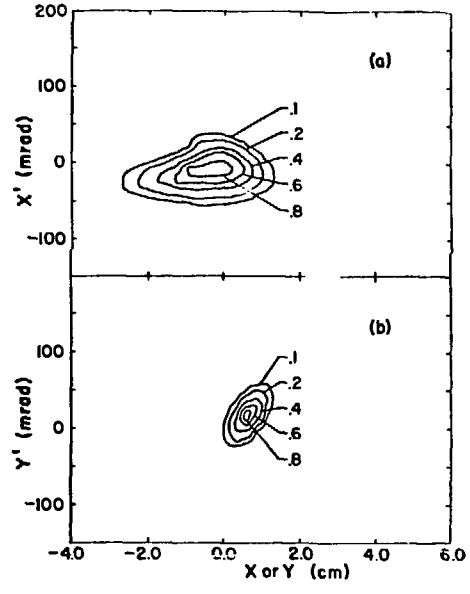

Fig. 8

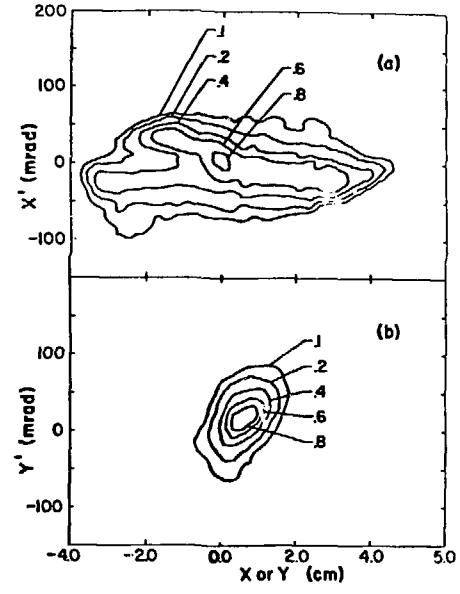

Fig. 9

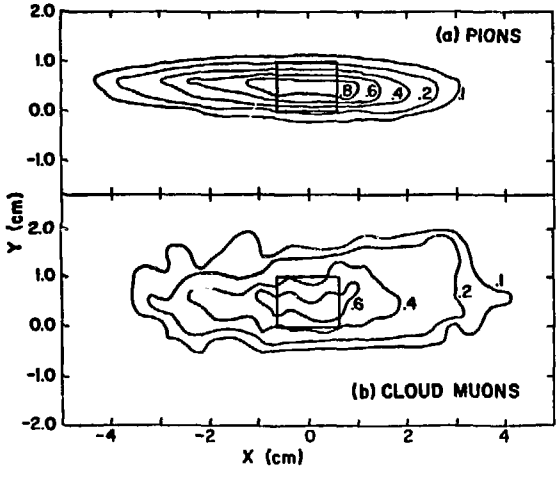

Fig. 10

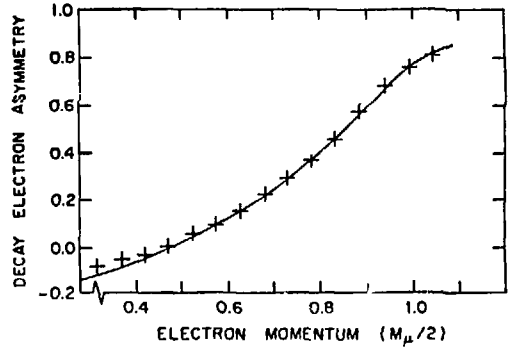

Fig. 11